CHINESE OPTICS LETTERS

Vol. 22, No. 10 | October 2024

Differential photoacoustic cell-based Fourier transform photoacoustic spectroscopy for background-free gas detection [Invited]

Xiaoli Liu (刘小利), Jiajia Cui (崔佳佳), Chaofan Feng (冯超凡), Qingyuan Tian (田清源), Ruyue Cui (崔茹悦), Yanting Zhao (赵延霆), Hongpeng Wu (武红鹏)*, and Lei Dong (董 磊)**

State Key Laboratory of Quantum Optics and Quantum Optics Devices, Institute of Laser Spectroscopy, Shanxi University, Taiyuan 030006, China

*Corresponding author: wuhp@sxu.edu.cn

**Corresponding author: donglei@sxu.edu.cn

Received June 4, 2024 | Accepted June 19, 2024 | Posted Online October 12, 2024

A broadband gas sensing technology is reported. The measurement principle relies on Fourier transform photoacoustic spectroscopy (FT-PAS) using a differential photoacoustic cell, in which both phase modulation and amplitude modulation are simultaneously applied to the broadband light sources. The thermal light source and supercontinuum source are employed sequentially. The performance of the FT-PAS is demonstrated by measuring the spectra of methane in the 2–10 μm range and acetylene in the 1–2 μm range. By leveraging the wavelength-independent nature of the photoacoustic effect, this system holds promise for comprehensive full-spectrum spectral detection.

Keywords: Fourier transform photoacoustic spectroscopy; gas sensing; broadband light source.
DOI: 10.3788/COL202422.101203

1. Introduction

Fourier transform photoacoustic spectroscopy (FT-PAS) is a high-sensitivity spectroscopic analysis method that combines background-free characteristics and high sensitivity of the photoacoustic effect with the wide spectral span of Fourier transform spectroscopy[1]. It is widely used in environmental monitoring, biomedicine, industrial process control, and materials science[2-4]. FT-PAS serves as a powerful analytical tool for the qualitative and quantitative analysis of gases, offering significant support for scientific research and practical applications. Moreover, the use of a Fourier transform spectrometer allows for a wide spectral range, making it suitable for the detection of various gases and the simultaneous detection of multi-component gas mixtures.

The principle of FT-PAS involves several key steps. (i) A broadband light source is phase-modulated by an interferometer, with additional amplitude modulation sometimes required[5]. (ii) The modulated light is directed at sample gas, where the sample absorbs light at specific frequencies, leading to periodic heating. This results in the thermal expansion and contraction of the surrounding gas, generating sound waves. (iii) The sound waves are detected by a microphone or pressure sensor, which converts the sound wave signals into electrical signals. (iv) The electrical signals are transmitted to a data processing system, where Fourier transform is performed. The Fourier transform converts the time-domain signals into frequency-domain signals, achieving the absorption spectrum of the sample. In traditional FT-PAS technology, a scanning interferometer modulates each wavenumber of the broadband light source at a distinct acoustic frequency $f = 2\nu v$ (ν is wavenumber, v is the scanning velocity). Consequently, a non-resonant acoustic detection module must be employed[6–8]. Resonant photoacoustic cells can amplify sound waves, enhancing the sensitivity of FT-PAS systems. Liu *et al.*[9–11] utilized two identical T-shaped photoacoustic cells placed in identical optical paths and adopted a differential mode to achieve signal amplification and noise suppression. However, this approach has certain limitations, including large system size and the critical challenge of ensuring identical resonant frequencies for the photoacoustic cells. When the resonant frequencies differ, it complicates the modulation of light and results in suboptimal signal amplification and incomplete noise suppression.

In this Letter, a differential photoacoustic cell (DPAC), structured as a dual-channel acoustic resonator, was utilized. For excitation sources, a broadband tungsten halogen lamp was used to detect methane (CH_4), while a supercontinuum (SC) source was employed to detect acetylene (C_2H_2). It has been shown that the DPAC can be integrated with a Fourier transform spectroscopy system. Moreover, the successful use of both coherent and incoherent light sources confirms the compatibility of the

FT-PAS system with various light sources. Considering the wavelength-independent nature of the photoacoustic effect[12], FT-PAS is expected to be compatible with light sources across a wide range, from ultraviolet (UV) to infrared (IR) and even terahertz (THz) bands, thereby enabling full-spectrum detection.

2. Experimental Setup

The schematic diagram of the FT-PAS system is shown in Fig. 1(a). Due to the use of a resonant photoacoustic cell, amplitude modulation at the resonant frequency of the photoacoustic cell was introduced to uniformly modulate all frequency components of the broadband light source. The broadband light source, after being amplitude modulated by the chopper and phase modulated by the Michelson interferometer, was shaped and directed into the DPAC to interact with the target gas. The mixed photoacoustic signal generated by absorbing the broadband light source was differentially detected by two microphones and then sent to a lock-in amplifier for 1f demodulation. The demodulated signal was converted from analog to digital and transmitted to a personal computer for Fourier transform processing to obtain the broadband absorption spectrum of the target gas.

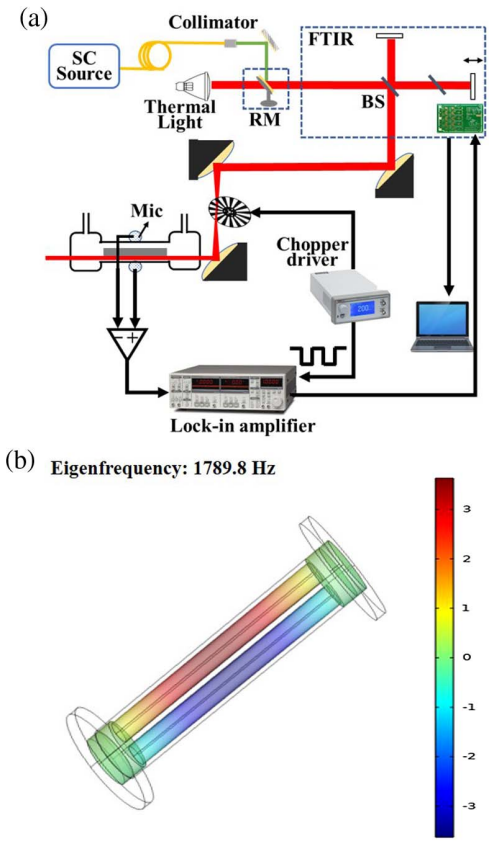

Fig. 1. (a) Diagram of the FT-PAS experimental setup: FTIR, Fourier transform infrared spectrometer; BS, beam splitter mirror; RM, reversible mirror; Mic: microphone; SC source, supercontinuum source. (b) Simulation diagram of DPAC.

The DPAC comprises two identical cylindrical acoustic resonators, with both ends connected by two buffer chambers (Φ20 × 10 mm). The length and diameter of each cylindrical resonator are 90 mm and 8 mm, respectively[13–15]. The excitation light beam travels through one of the acoustic resonators, generating sound waves that resonate within the symmetrical dual-channel resonators. Two identical microphones are mounted on the middle arms of the resonators, where the sound pressure amplitude is highest, to detect the sound waves. The DPAC operates at its resonant frequency, where the gas moves like a piston, compressing in one chamber while expanding in the other. This results in the pressure in the two acoustic resonators oscillating in opposite phases, creating sound field amplitudes that are equal but with opposite phases. In this configuration, background noise from the window, external environmental disturbances, flow noise, and other noise components generated as the gas passes through the photoacoustic cell remain in phase. Consequently, the amplitude of the photoacoustic signal can be doubled by subtracting the signals collected by the microphones in the dual-channel resonators, while noise can be effectively suppressed[16]. The simulation in Fig. 1(b) illustrates the distribution characteristics of the acoustic field inside the DPAC. The measured resonant frequency and Q factor of the DPAC were 1779.8 Hz and 47, respectively, in air. The resonant frequency is in excellent agreement with the simulation result of 1789.8 Hz. A reversible mirror was used to redirect the excitation light source, which included the tungsten halogen lamp or SC source (YSL, SC-5-FC).

3. Results and Discussion

When the moving mirror in the Michelson interferometer reaches the position of the optical path difference δ, the signal $S(\delta)$ generated within the photoacoustic cell can be expressed as[10,17]

$$S(\delta) = KI(\delta)N_{\mathrm{tot}}c\sigma(\nu), \tag{1}$$

where K represents the constant of the photoacoustic cell, which characterizes the ability of the photoacoustic cell in the FT-PAS system to convert the absorbed incident light into the output electrical signal through thermal, acoustic, and electrical forms, $I(\delta)$ represents the output light intensity of the interferometer at an optical path difference of δ, N_{tot} represents the total number density of gas molecules per unit volume, c is the concentration of the target gas, and $\sigma(\nu)$ is the absorption cross-section of target gas at wavenumber ν. The detected electrical signal $S(\delta)$, depicted as an interference pattern in the time domain, and the FT-PAS signal $B(\nu)$ associated with wavenumber ν are yielded by Fourier transform processing $S(\delta)$,

$$B(\nu) = 2KN_{\mathrm{tot}}c\sigma(\nu) \times \int_0^{\infty} I(\delta)\cos(2\pi\delta\nu)\mathrm{d}\delta. \tag{2}$$

Firstly, the broadband tungsten halogen lamp with a spectral range from 1000 cm^{-1} to 10,000 cm^{-1} was chosen as the excitation light source of the FT-PAS system to verify the feasibility of the FT-PAS system. A mixture gas of 1% CH_4 and nitrogen (N_2) filled the DPAC, and measurements were carried out using the DPAC-based FT-PAS system. Figure 2(a) shows the FT-PAS CH_4 spectrum, and three absorption bands of 1% CH_4 are prominent at about 1299.8, 3016.3, and 4215.8 cm^{-1}, respectively. The detection result demonstrates the broad spectrum and multiplex advantage of FT-PAS technology, enabling the capture of all absorption bands of methane gas within the spectral range of the light source and obtaining a complete broadband absorption spectrum in a single measurement. An optical aperture (not shown in the system diagram) was inserted into the optical path to adjust the incident power into the photoacoustic cell, and 1% CH_4 gas was successively detected at various power levels. The peak values around 3016.3 cm^{-1} and 4215.8 cm^{-1} were extracted to derive the response of the FT-PAS signals to power, as shown in Fig. 2(b). The results illustrate that the FT-PAS signal is directly proportional to the power, consistent with characteristic behavior of the photoacoustic effect. The power spectrum of the tungsten halogen lamp at 1299.8 cm^{-1} is approximately 5 times weaker than that at 3016.3 cm^{-1}. This precisely elucidates why the signal appears weak around 1299.8 cm^{-1}, despite the CH_4 absorption band intensity being only half as strong as that around 3016.3 cm^{-1}.

The power shown in Fig. 2(b) represents the total power of the thermal light source incident into the photoacoustic cell. When the total incident power reaching the photoacoustic cell is 1.84 mW, the powers at the absorption bands near 3016.3 cm^{-1} and 4215.8 cm^{-1} were approximately 167 μW and 242 μW, respectively, as calculated from the emission power spectrum of the broadband light source.

The aperture diameter was set to a fixed size to ensure that the total power incident into the photoacoustic cell was 1.84 mW. Methane gas concentrations ranging from 2000 to 7500 ppm (parts per million) were obtained by diluting 1% CH_4 with N_2 and were subsequently detected. The relationship between the FT-PAS signal and the concentration was determined, as shown in Fig. 3. Due to strong absorption around 3016.3 cm^{-1}, nonlinearity in absorption occurred. However, at the weak absorption line of 4215.8 cm^{-1}, the FT-PAS system exhibited good linearity. Therefore, it is believed that the FT-PAS signal's dependence on low concentrations of CH_4 at 3016.3 cm^{-1} also shows good linearity. This demonstrates that the system has a very wide dynamic range of concentrations. The signal fluctuations of N_2 were taken as the noise floor (1σ) of the FT-PAS system. The signal-to-noise ratio (SNR) for 3000 ppm CH_4 was calculated by dividing the peak signal value by the 1σ value of the standard deviation, resulting in an SNR of 34 around 4219.7 cm^{-1} and 497 around 3016.3 cm^{-1}. This corresponds to CH_4 detection limits of 87 ppm and 6 ppm, respectively.

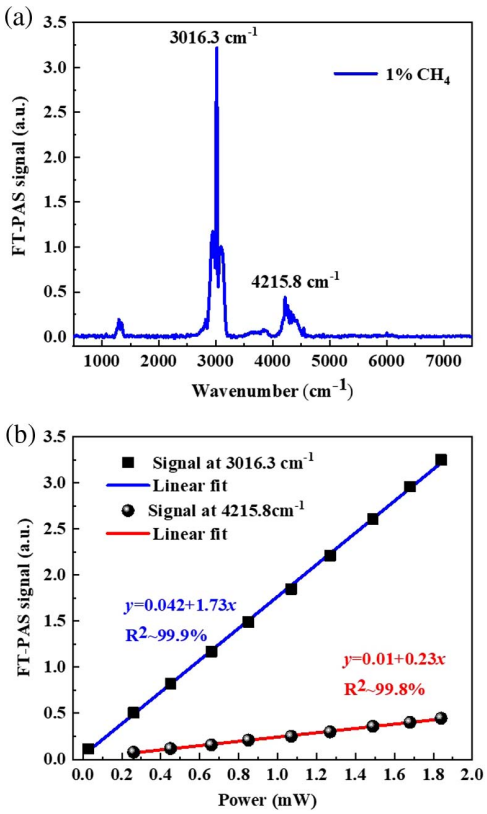

Fig. 2. (a) FT-PAS spectrum of 1% CH_4. (b) Dependency of the FT-PAS amplitude peak on the incident light power.

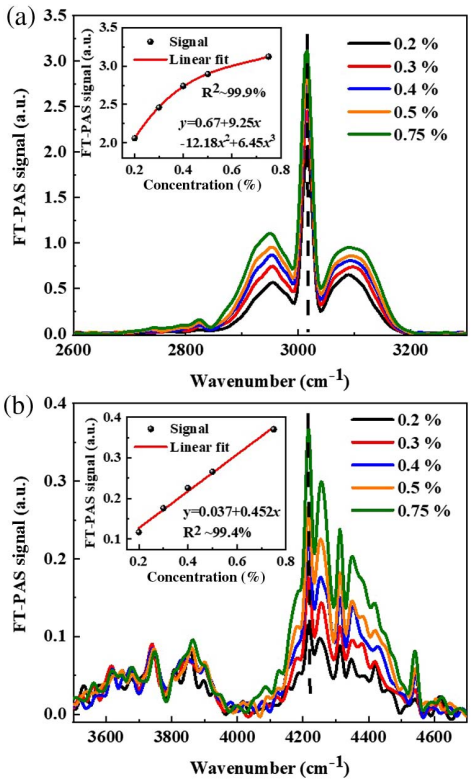

Fig. 3. FT-PAS spectra of CH_4 gas. (a) CH_4 FT-PAS spectra of various concentrations around 3016.3 cm^{-1}. (b) CH_4 FT-PAS spectra of various concentrations around 4215.8 cm^{-1}.

The above measured spectra of CH_4 covered the 2–10 μm band. To verify the FT-PAS system's response within the 1–2 μm band, an SC source with a wavelength from 480 nm to 2200 nm, characterized by high power density and good beam quality, was selected as the excitation light source. Given that the thermal light source has a very weak emission spectrum in the 1–2 μm band [shown in Fig. 4(a)], where the gas absorption is also relatively weak, integrating the SC source into the FT-PAS system will demonstrate its compatibility with a wider range of light source.

C_2H_2 gas was detected by the FT-PAS system. Figure 4(b) shows the FT-PAS spectrum of 1% C_2H_2, where two absorption bands are observed. The power of the emitted light was adjusted by changing the drive current of the SC source. The relationships between the peak values of two absorption bands and the incident light power were studied. The results, as shown in Fig. 5(a), indicate that the signal peaks of the FT-PAS exhibit good linearity.

Finally, the incident light power into the DPAC was fixed at 2.3 mW. Samples of C_2H_2 gas with concentrations in the range of 3000–7500 ppm were measured, and the FT-PAS peak values around 6580.3 cm^{-1} were plotted against concentration in Fig. 5(b). The experimental data, fitted with a linear model, exhibited the expected linear dependence on the C_2H_2 concentration. Therefore, the feasibility of the FT-PAS system based on a resonant photoacoustic cell compatible with different light sources has been demonstrated. This is highly significant for future detections and applications of THz light sources.

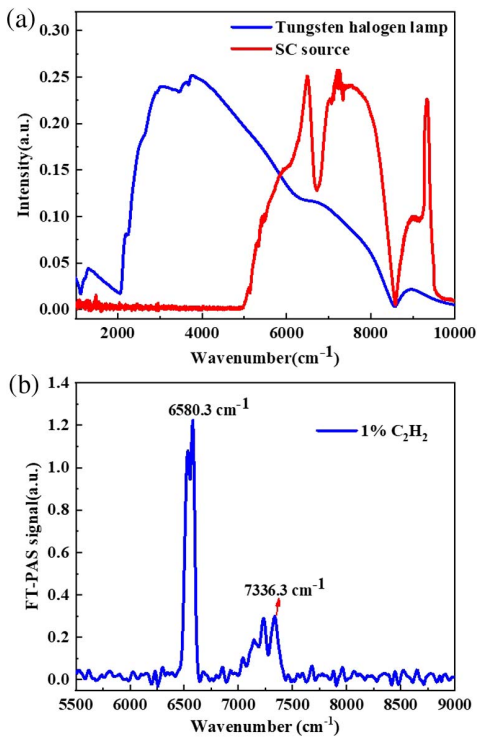

Fig. 4. (a) Emission power spectra of the tungsten halogen lamp and SC source. (b) FT-PAS spectrum of 1% C_2H_2.

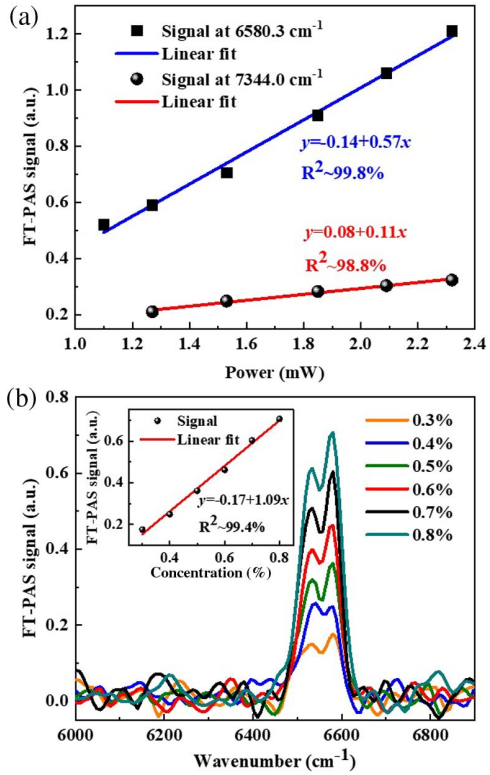

Fig. 5. (a) Dependency of 1% C_2H_2 FT-PAS amplitude peak on the power. (b) C_2H_2 FT-PAS spectra around 6580.3 cm^{-1} as a function of concentration.

4. Conclusion

In conclusion, a broadband gas optical sensing technology based on FT-PAS and a DPAC has been validated across the 1–10 μm band. In addition to the phase modulation applied by the scanning interferometer, as in traditional FT-PAS system, amplitude modulation via a mechanical chopper is also required to modulate all wavenumbers of the light source to induce resonance in the DPAC. Using a tungsten halogen lamp as the thermal light source, we measured the complete spectra of CH_4 in the 2–10 μm range and achieved a detection limit of 6 ppm. Then an SC broadband light source was employed for C_2H_2, and the characteristic spectra of C_2H_2 in the 1–2 μm range were obtained. This technology is expected to achieve full-spectrum detection, which has significant implications for the THz domain. Furthermore, given super-continuous spectral response characteristics of quartz tuning fork spectroscopy sensing techniques[18–20], combining these with FTS technology is expected to greatly facilitate broadband detection and multi-gas detection across the entire spectral range.

Acknowledgements

This work was supported by the National Natural Science Foundation of China (NSFC) (Nos. 62235010, 62175137, 62122045, and 62075119), Shanxi Science Fund for Distinguished Young Scholars (No. 20210302121003), and

Shanxi Provincial Special Fund for Scientific and Technological Cooperation and Exchange (No. 202304041101019).

References

1. C. B. Hirschmann, J. Uotila, S. Ojala, *et al.*, "Fourier transform infrared photoacoustic multicomponent gas spectroscopy with optical cantilever detection," Appl. Spectrosc. **64**, 293 (2010).
2. J. Huang, G. Bekiaris, T. Fitamo, *et al.*, "Prediction of biochemical methane potential of urban organic waste using Fourier transform mid-infrared photoacoustic spectroscopy and multivariate analysis," Sci. Total Environ. **790**, 147959 (2021).
3. C. B. Hirschmann, N. S. Koivikko, J. Raittila, *et al.*, "FT-IR-cPAS—new photoacoustic measurement technique for analysis of hot gases: a case study on VOCs," Sensors **11**, 5270 (2011).
4. J. F. McClelland, R. W. Jones, S. Luo, *et al.*, *A Practical Guide to FTIR Photoacoustic Spectroscopy* (CRC Press, 1993).
5. L. X. Liu, A. Mandelis, A. Melnikov, *et al.*, "Step-scan T-cell Fourier transform infrared photoacoustic spectroscopy (FTIR-PAS) for monitoring environmental air pollutants," Int. J. Thermophys. **37**, 64 (2016).
6. J. Karhu, T. Tomberg, F. Senna Vieira, *et al.*, "Broadband photoacoustic spectroscopy of $^{14}CH_4$ with a high-power mid-infrared optical frequency comb," Opt. Lett. **44**, 1142 (2019).
7. T. Mikkonen, C. Amiot, A. Aalto, *et al.*, "Broadband cantilever-enhanced photoacoustic spectroscopy in the MIR-IR using a supercontinuum," Opt. Lett. **43**, 5094 (2018).
8. M. Zhang, B. Zhang, K. Chen, *et al.*, "Miniaturized multi-pass cell based photoacoustic gas sensor for parts-per-billion level acetylene detection," Sens. Actuators A Phys. **308**, 112013 (2020).
9. L. X. Liu, H. T. Huan, A. Mandelis, *et al.*, "Design and structural optimization of T-resonators for highly sensitive photoacoustic trace gas detection," Opt. Laser Technol. **148**, 107695 (2022).
10. L. X. Liu, A. Mandelis, H. T. Huan, *et al.*, "Step-scan differential Fourier transform infrared photoacoustic spectroscopy (DFTIR-PAS): a spectral deconvolution method for weak absorber detection in the presence of strongly overlapping background absorptions," Opt. Lett. **42**, 1424 (2017).
11. Q. Huang, Y. Wei, and J. S. Li, "Simultaneous detection of multiple gases using multi-resonance photoacoustic spectroscopy," Sens. Actuators B Chem. **369**, 132234 (2022).
12. H. D. Zheng, L. Dong, A. Sampaolo, *et al.*, "Overtone resonance enhanced single-tube on-beam quartz enhanced photoacoustic spectrophone," Appl. Phys. Lett. **109**, 111103 (2016).
13. X. K. Yin, H. P. Wu, L. Dong, *et al.*, "Ppb-level SO_2 photoacoustic sensors with a suppressed absorption–desorption effect by using a 7.41 μm external-cavity quantum cascade laser," ACS Sensors **5**, 549 (2020).
14. H. D. Zheng, M. H. Lou, L. Dong, *et al.*, "Compact photoacoustic module for methane detection incorporating interband cascade light emitting device," Opt. Express **25**, 16761 (2017).
15. H. D. Zheng, Y. H. Liu, H. Y. Lin, *et al.*, "Sub-ppb-level CH_4 detection by exploiting a low-noise differential photoacoustic resonator with a room-temperature interband cascade laser," Opt. Express **28**, 19446 (2020).
16. X. L. Liu, H. P. Wu, and L. Dong, "Methodology and applications of acousto-electric analogy in photoacoustic cell design for trace gas analysis," Photoacoustics **30**, 100475 (2023).
17. L. X. Liu, A. Mandelis, H. T. Huan, *et al.*, "Step-scan T cell-based differential Fourier transform infrared photoacoustic spectroscopy (DFTIR-PAS) for detection of ambient air contaminants," Appl. Phys. B **122**, 268 (2016).
18. A. Sampaolo, P. Patimisco, M. Giglio, *et al.*, "Improved tuning fork for terahertz quartz-enhanced photoacoustic spectroscopy," Sensors **16**, 439 (2016).
19. L. G. Xu, S. Zhou, N. W. Liu, *et al.*, "Multigas sensing technique based on quartz crystal tuning fork-enhanced laser spectroscopy," Anal. Chem. **92**, 14153 (2020).
20. J. P. Wang, H. P. Wu, A. Sampaolo, *et al.*, "Quartz-enhanced multiheterodyne resonant photoacoustic spectroscopy," Light Sci. Appl. **13**, 77 (2024).